

Oriental quantum revivals of nanoscale rotors

Benjamin A. Stickler,¹ Birthe Papendell,¹ Stefan Kuhn,² James Millen,² Markus Arndt,² and Klaus Hornberger¹

¹University of Duisburg-Essen, Faculty of Physics, Lotharstraße 1, 47048 Duisburg, Germany

²University of Vienna, Faculty of Physics, VCQ, Boltzmannngasse 5, 1090, Vienna, Austria

We propose an experimentally viable scheme to probe orientational quantum revivals with nanoscale particles, an interference effect of the rotational degrees of freedom testifying a superposition of all orientations. Our simulations demonstrate that such revivals are observable with current technology, even in the presence of environmental decoherence, using carbon nanotubes or silicon nanorods with a length of 50 nm. This opens the door to tests of rotational quantum physics with submicron objects and to quantum gyroscopic torque sensors.

Introduction — The rapidly growing field of optomechanics offers a promising platform for quantum technology [1] and fundamental tests of quantum theory [2]. While the mechanical motion of picogram cantilevers has been cooled into the quantum regime [3–5], their dynamics is still affected by clamping losses and decoherence. An attractive way to minimize such environmental disturbances is to levitate and cool the motion of a nanoparticle in high vacuum [6–8].

The successful optical cavity and feedback cooling of levitated nanospheres to millikelvin temperatures and below [9–14], enables high precision force sensing [15, 16] and renders the quantum regime a realistic goal for the near future [6–8]. By switching off the trapping fields, the state of a levitated particle disperses freely, paving the way for free fall quantum experiments with massive spherical particles [17, 18]. Using anisotropic objects instead of spheres enhances the optical interaction and cooling rates [19, 20] and has the benefit that the orientational degrees of freedom can be exploited for high-precision torque sensing [20–24] and quantum experiments [25–30].

Here, we propose a quantum experiment probing the superposition and collective interference of all orientations of a nanoscale particle. It exploits the fact that an initially tightly oriented quantum rotor quickly disperses into a superposition of all orientations. Only at multiples of a quantum revival time their collective interference leads to a complete reappearance of the initial state [31]. Such *orientational quantum revivals* are an inherently rotational interference effect caused by the quantization of angular momentum. They have been observed in dense gases of small molecules as the recurrence of alignment following a strong laser pulse [32, 33].

We find that the orientational quantum revivals of an initially aligned rotor with a length of tens of nanometers can be observed under feasible experimental conditions. Surprisingly, the presented scheme works for moderate initial temperatures, with several thousand angular momentum quanta occupied, and under realistic environmental conditions, taking into account all relevant sources of orientational decoherence. It requires only a single nanoparticle, which is recycled during the experiment. The observation of orientational quantum revivals will provide the first experimental test of nanoscale ori-

entational coherences, paving the way for quantum coherent gyroscopic torque sensing.

Outline — The proposed scheme consists of repeating the four consecutive steps displayed in Fig. 1: (a) alignment, (b) dispersion, (c) revival, and (d) recapture. After discussing each step in detail we estimate the decoherence rates due to scattering of residual gas atoms and thermal photon emission for carbon nanotubes and silicon nanorods. Our simulation of the expected alignment signal demonstrates that the observation of such revivals is a challenging but achievable goal.

We consider a nanoscale linear rigid rotor of length ℓ , mass M , and moment of inertia $I = M\ell^2/12$ levitated in high vacuum by an optical tweezer, consisting of two counter-propagating beams of power P and polarization direction $\boldsymbol{\varepsilon}$, which form a standing wave of waist w . The tweezer is aligned with the gravitational field so that the particle drops along the tweezer axis. Denoting the angle between the rotor symmetry axis and $\boldsymbol{\varepsilon}$ by β , the optical potential of the nanoparticle orientation at the antinode is given by $V(\beta) = -V_0 \cos^2 \beta$. The potential depth is $V_0 = 4\Delta\alpha P/\pi c\epsilon_0 w^2$ with the polarizability anisotropy $\Delta\alpha = \alpha_{\parallel} - \alpha_{\perp}$.

Alignment — The orientation of the nanoparticle can be cavity or feedback cooled [19, 34] leading to a tight alignment of the rotor with the field polarization direction. The quantum state of the rotor is then characterized by its rotational temperature T and takes the form $\rho_0 = \exp(-H/k_B T)/Z$ with the Hamiltonian $H = \mathbf{J}^2/2I + V(\beta)$ and the partition function Z , where \mathbf{J} is the angular momentum operator. Operators are denoted by sans serif characters.

The matrix elements of the initial state in the angular momentum basis $|jm\rangle$ (with $\hbar m$ the angular momentum component along the field polarization) can be evaluated numerically by exact diagonalization of H . In the semiclassical regime, where millions of angular momentum states are occupied, exact diagonalization becomes intractable. Using Bohr-Sommerfeld quantized action-angle variables [35] the semiclassical matrix elements can

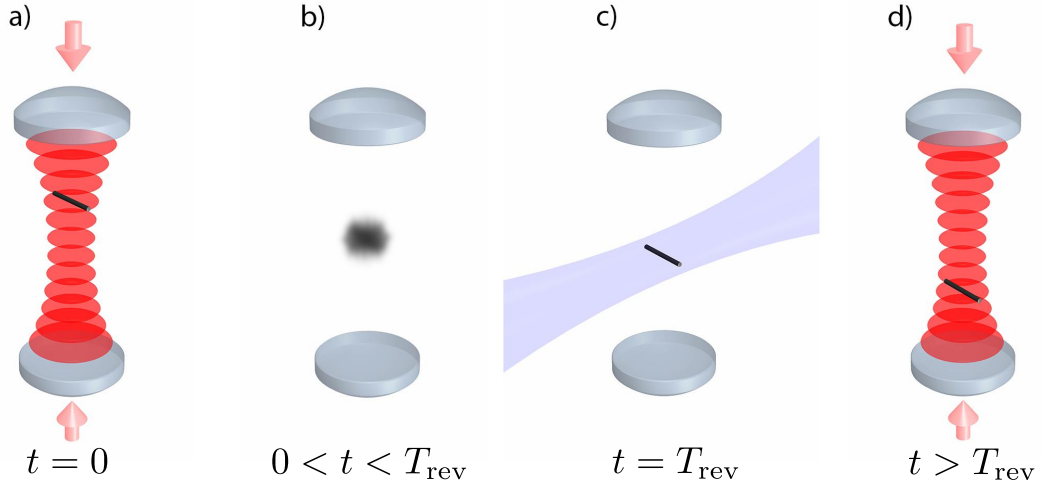


Figure 1. Scheme to observe orientational quantum revivals of a nanoscale rotor. (a) The rotor is levitated in an optical tweezer formed by two counter-propagating laser beams. Cavity or feedback cooling to subkelvin temperatures tightly aligns it with the field polarization. (b) After switching off the trapping and cooling laser the quantum state of the rotor quickly disperses into a superposition of all different orientations, while its center-of-mass drops in the gravitational field. (c) At integer multiples of the revival time T_{rev} all orientations interfere constructively so that the initial state is recovered. This *orientational quantum revival* is detected by the light scattered from a probe beam, which collapses the rotor into a state of definite orientation. (d) To repeat this quantum measurement several times, the rotor is recaptured with the trapping lasers and then transferred back by tuning their relative phase.

be calculated as (see Appendix A)

$$\begin{aligned} \langle jm | \rho_0 | j'm' \rangle &\simeq \frac{\delta_{mm'}}{Z} I_{\frac{j-j'}{2}} \left[\frac{V_0}{2k_B T} \left(1 - \frac{4m^2}{(j+j'+1)^2} \right) \right] \\ &\times \exp \left[\frac{V_0}{2k_B T} \left(1 - \frac{4m^2}{(j+j'+1)^2} \right) \right] \\ &\times \exp \left[-\frac{\hbar^2(j+j'+1)^2}{8Ik_B T} \right] \end{aligned} \quad (1)$$

for $j - j'$ even and $\langle jm | \rho_0 | j'm' \rangle = 0$ otherwise. Here, $I_n(\cdot)$ denotes the modified Bessel function. The expectation value of the total angular momentum quantum number can be approximated as (see Appendix A) $\langle j \rangle_0 \simeq \sqrt{\pi k_B T I / 2 \hbar^2}$, yielding occupations as large as $\langle j \rangle_0 \simeq 8.2 \times 10^3$ for $\ell \simeq 50$ nm, $M \simeq 10^5$ amu, and $T = 1$ K.

The initial orientational alignment can be quantified by the expectation value $\langle \cos^2 \beta \rangle_0 = \text{tr}(\rho_0 \cos^2 \beta)$, from now on referred to as the *alignment*. It is unity for a perfectly aligned particle and $1/3$ for uniformly distributed orientations. For the initial state (1) the alignment can be determined in leading order of $k_B T / V_0$ as (see Appendix A)

$$\langle \cos^2 \beta \rangle_0 = k_B T \frac{\partial}{\partial V_0} \ln Z \simeq 1 - \frac{k_B T}{V_0}. \quad (2)$$

This relation holds if many angular momentum quanta are occupied (but fails in the deep quantum regime where the alignment is limited by the uncertainty relation).

Alignment dynamics during free fall— Once the trapping laser is turned off, the orientation state evolves

freely while its center of mass drops in the gravitational field along the tweezer axis. The ensuing delocalization of the orientation state is counteracted by orientational decoherence processes [36–38] which potentially suppress the revivals. As in other matter wave experiments [17, 18, 39–42], the dominant sources of environmental decoherence are the scattering of residual gas atoms and the thermal emission of photons.

As a very conservative estimate, we assume that a single decoherence event suffices to completely erase the acquired orientational coherences by producing an isotropic state $\rho_i \propto \exp(-\lambda_i \mathbf{H}_0)$ with $\mathbf{H}_0 = \mathbf{J}^2 / 2I$. The rotor dynamics can then be described by the Markovian master equation $\partial_t \rho = -i[\mathbf{H}_0, \rho] / \hbar + \Gamma(\rho_i - \rho)$, where Γ is the total rate of decoherence events. The state $\rho(t)$ at time t is thus given by

$$\rho(t) = \rho_u(t) e^{-\Gamma t} + \rho_i (1 - e^{-\Gamma t}), \quad (3)$$

where $\rho_u(t)$ is the unitary evolution with matrix elements

$$\begin{aligned} \langle jm | \rho_u(t) | j'm' \rangle &= \sum_{j,j'=0}^{\infty} \sum_{m=-j}^j \sum_{m'=-j'}^{j'} \langle jm | \rho_0 | j'm' \rangle \\ &\times \exp \left[-\frac{i\hbar t}{2I} [j(j+1) - j'(j'+1)] \right]. \end{aligned} \quad (4)$$

The alignment $\langle \cos^2 \beta \rangle = \text{tr}[\rho(t) \cos^2 \beta]$ at time t is independent of λ_i and given by

$$\langle \cos^2 \beta \rangle = \langle \cos^2 \beta \rangle_u e^{-\Gamma t} + \frac{1}{3} (1 - e^{-\Gamma t}), \quad (5)$$

where $\langle \cos^2 \beta \rangle_{\text{u}}$ denotes the alignment dynamics of the decoherence-free evolution (see Appendix A).

The initially trapped orientation state quickly disperses during free fall due to its angular momentum spread. This rapid alignment decay can be approximated using the shearing dynamics associated with a flat orientation space (see Appendix A),

$$\langle \cos^2 \beta \rangle_{\text{u}} \simeq \langle \cos^2 \beta \rangle_0 e^{-\kappa^2 t^2} + \frac{1}{2} \left(1 - e^{-\kappa^2 t^2} \right), \quad (6)$$

with rate $\kappa = \sqrt{2k_{\text{B}}T/I}$. The width and height of the orientational quantum revival are determined by the initial rotational temperature as described by Eqs. (2) and (6).

The corresponding classical dynamics exhibits the same alignment decay since ρ_0 is virtually indistinguishable from a classical thermal state for the considered temperatures. After this initial alignment reduction to a value of $1/2$, the classically expected alignment signal shows no revivals at all. Rather, it decays as $1/3 + e^{-\Gamma t}/6$, based on the same assumptions that lead to (5).

The alignment of the quantized rotor follows this classical prediction for most of the times. However, the initial orientation state (2) completely recurs at integer multiples of the revival time $T_{\text{rev}} = 2\pi I/\hbar$, as follows directly from (4) and as displayed in Fig. 2 (see below). These quantum revivals are a genuine quantum interference effect based on angular momentum quantization [31], testifying a superposition of all orientation states.

Measuring the alignment — The alignment of the rotor can be directly extracted by light scattering from a running wave probe beam. Choosing its polarization in the same direction as that of the trapping laser, the scattered light intensity is proportional to the alignment $\cos^2 \beta$ [19, 43].

The scattering of probe photons decoheres the rotor state to a definite orientation, implementing a quantum measurement of $\cos^2 \beta$. By probing the particle orientation after variable times t in repeated experimental runs one can thus test for the emergence of orientational revivals. It is beneficial to repeat the experiment with the same rotor in order to reduce the requirements on nanoparticle fabrication and characterization.

Recapture — In the final step of the scheme the rotor is recaptured by switching on the trapping laser when the particle traverses an antinode. Moderate laser powers of a few Watts suffice for a nanoparticle of length $\ell = 50$ nm and mass $M = 10^5$ amu. For such particles the revival time is as short as $T_{\text{rev}} \simeq 2$ ms so that the rotor drops only $20 \mu\text{m}$ and reaches the center-of-mass velocity 20 mm/s. For longer revival times, it can be beneficial to use the detection laser rather than the trapping laser for recapturing the rotor, which can then be transferred into the trap in an additional step.

Orientalional Decoherence Rates — The total decoherence rate Γ accounts for collisions with residual gas atoms and for the emission of thermal photons, $\Gamma = \Gamma_{\text{gas}} + \Gamma_{\text{emi}}$.

The rate at which thermal gas atoms of mass m_{g} , pressure p_{g} , and temperature T_{g} scatter off a cylinder of length ℓ and diameter d can be obtained by integrating the mean particle flux into the surface over the particle shape

$$\Gamma_{\text{gas}} = \frac{\pi p_{\text{g}} d \ell}{\sqrt{2\pi m_{\text{g}} k_{\text{B}} T_{\text{g}}}} \left(1 + \frac{d}{2\ell} \right). \quad (7)$$

The rate of thermally emitted photons depends on the internal temperature and the material-specific spectral absorption cross section of the nanoparticle [18, 44]. The former is determined by the heating of the particle during the recycling and alignment step. The effect of heating can be minimized by choosing the infrared wavelength of the trapping laser between vibrational transitions, where the particle is practically transparent.

Carbon Nanotubes and Silicon Nanorods — To demonstrate the viability of the proposed scheme, we discuss the experimental realization for two types of nanoscale rotors, semiconducting double-walled carbon nanotubes (CNTs) and silicon nanorods (SNRs). Both can be fabricated with a length of $\ell = 50$ nm, implying that the CNTs have a mass of $M = 1.9 \times 10^5$ amu (outer diameter $d = 1.5$ nm, inner diameter 1.0 nm) while the SNRs have a mass of $M = 1.4 \times 10^6$ amu ($d = 5$ nm). The resulting revival times are $T_{\text{rev}} \simeq 3.8$ ms and $T_{\text{rev}} \simeq 28$ ms, respectively, implying that the particles fall about $72 \mu\text{m}$ and 4.0 mm per revival. The polarizability anisotropy of CNTs is taken from Ref. [45], and that of SNRs is determined as in Refs. [19, 43].

The nanoparticle is initially trapped in an optical tweezer of waist $w = 30 \mu\text{m}$ and power $P = 5$ W. For SNRs it has been demonstrated in Ref. [18] that internal heating and photon emission is negligible for a wavelength of $1.55 \mu\text{m}$. For CNTs, where excitonic excitations play no role for wavelengths well above $2.5 \mu\text{m}$ [46], the exact position and width of the vibrational excitations depends on the structural details of the particle [47] and the optimal trapping wavelength can be determined experimentally.

Cavity or feedback cooling the rotation of the trapped particles to subkelvin temperatures is feasible [19, 34] but may require low mode volume cavities [48] to enhance the nanoparticle-light interaction and detection efficiency. The deeply trapped particle is harmonically bound, so that well established techniques of center-of-mass optical cooling can be exploited [6–14].

Figure 2 shows the expected scattering signal for CNTs as a function of the time delay between nanoparticle release and detection. The alignment approaches a minimum at all half integer multiples of T_{rev} , a quantum effect related to the angular momentum parity of the initial state, and decays on the timescale $1/\Gamma \simeq 145$ ms due to collisional decoherence at $p_{\text{g}} = 10^{-8}$ mbar. The initial state is determined by exact numerical diagonalization of \mathbf{H} , involving several thousand total angular momentum quanta. The expected signal for SNRs displays a similar structure, as shown in Appendix A.

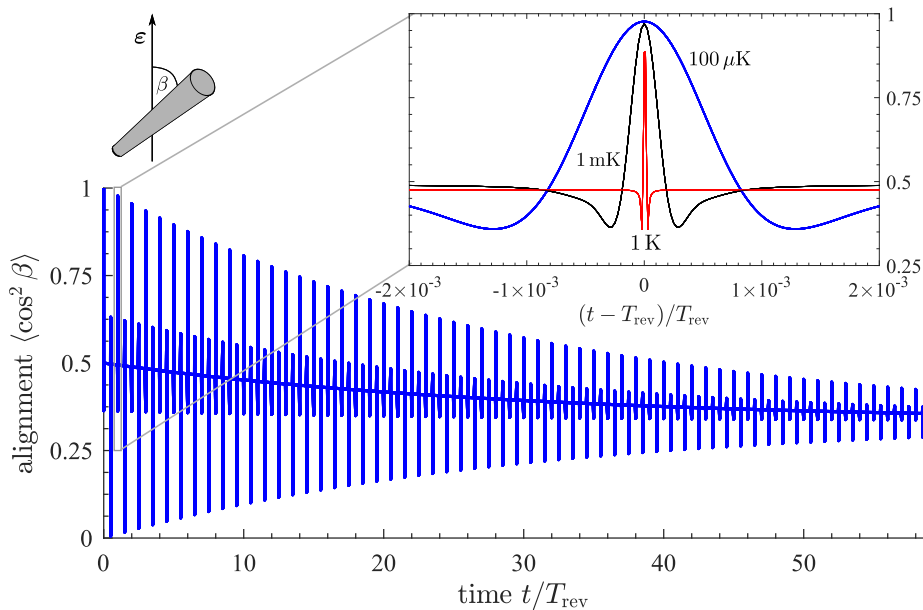


Figure 2. Orientational alignment $\langle \cos^2 \beta \rangle$ signal of carbon nanotubes ($m = 1.9 \times 10^5$ amu, $\ell = 50$ nm) as a function of time (blue solid line) for $T = 100 \mu\text{K}$. For most of the time, the alignment decays exponentially with decoherence rate Γ from $1/2$ towards $1/3$. However, the initial alignment recurs at integer multiples of the revival time $T_{\text{rev}} = 2\pi I/\hbar \simeq 3.8$ ms and approaches a minimum at half integer multiples of T_{rev} . The inset shows the first such orientational quantum revival for three different initial temperatures. The width of the revival peak is determined by the decay time of the initial state, $1/\kappa = \sqrt{I/2k_B T}$. The initially trapped state is numerically calculated by exact diagonalization of \mathbf{H} and then propagated with (3). As explained after (6), the classically expected signal amounts to the quantum signal without the revival spikes around $t = nT_{\text{rev}}/2, n \in \mathbb{N}$.

Quantum Coherent Gyroscopic Sensors — The presence of an external torque during the free time evolution can have a strong influence on the orientational revival signal. By monitoring the alignment signal as a function of time for different initial orientations the magnitude and direction of an applied torque can thus be deduced. Denoting this magnitude by N_{max} a quantum coherent gyroscope will accumulate a phase on the order of $\varphi = N_{\text{max}}T_{\text{rev}}/\hbar$ within a single revival. Since phase shifts on the order of π already significantly reduce the quantum revival we find that torques as low as 10^{-31} Nm can be observed with carbon nanotubes, nine orders of magnitude better than the best classical setup considered so far [22]. The torque sensitivity can be further improved by measuring revivals at higher multiples of the revival time.

By attaching single elementary charges to the ends of the silicon nanorod discussed above one can measure electrostatic fields at the $\mu\text{V}/\text{m}$ level. The decay of the alignment signal when the rotor is exposed to an atomic beam or other controlled environments can be used for studying collisional decoherence and quantum thermalization of the nanoscale rotor. Finally, objective collapse models [49] can be ruled out by observing orientational quantum revival that contradict the predicted loss of orientational coherence [50].

Conclusion — We presented a viable scheme for the first observation of orientational quantum revivals of nanoscale particles. The proposed experiment can be re-

alized with current technology, opening the door to quantum enhanced torque sensing. The successful demonstration of orientational revivals may well be the starting point for interferometric manipulation methods of nanoscale rigid rotors, based on applying a sequence of optical potentials during the free evolution.

Acknowledgments — B.A.S. and B.P. contributed equally. This work was supported by the Deutsche Forschungsgemeinschaft (DFG, HO 2318/7-1) and by the Austrian Science Fund (FWF, P27297). S.K. acknowledges funding by the ESQ from the Austrian Academy of Science in the project ROTOQUOP.

Appendix A

1. Bohr-Sommerfeld Quantization

For completeness, we briefly summarize how to approximate quantum mechanical matrix elements of the linear rotor using Bohr-Sommerfeld quantization. The angles α, β and their canonical angular momenta p_α, p_β are related to the action-angle variables α_m, α_j, m, j via [M. S. Child, *Semiclassical mechanics with molecular applications*, Oxford University Press, 2014]

$$\alpha = \alpha_m + \arctan(\zeta \tan \alpha_j) - \pi \quad (\text{A1a})$$

$$\cos \beta = \cos \alpha_j \sqrt{1 - \zeta^2} \quad (\text{A1b})$$

$$\sin \beta = \sqrt{\sin^2 \alpha_j + \zeta^2 \cos^2 \alpha_j} \quad (\text{A1c})$$

$$p_\beta = \hbar \left(j + \frac{1}{2} \right) \frac{\sin \alpha_j \sqrt{1 - \zeta^2}}{\sqrt{\sin^2 \alpha_j + \zeta^2 \cos^2 \alpha_j}}, \quad (\text{A1d})$$

$$p_\alpha = \hbar m, \quad (\text{A1e})$$

with $\zeta = m/(j + 1/2)$. Note that these relations imply $p_\alpha^2/\sin^2 \beta + p_\beta^2 = \hbar^2(j + 1/2)^2$.

The matrix elements $\langle jm | \mathbf{A} | j'm' \rangle$ of an arbitrary operator $\mathbf{A} = A(\alpha, \beta, p_\alpha, p_\beta)$ can be semiclassically approximated by first replacing all arguments of A according to (A1), yielding $\bar{A}(\alpha_m, \alpha_j, m, j)$. The matrix elements can then be obtained by calculating

$$\langle jm | \mathbf{A} | j'm' \rangle \simeq \frac{1}{(2\pi)^2} \int_0^{2\pi} d\alpha_m \int_0^{2\pi} d\alpha_j e^{i\alpha_m(m-m')} e^{i\alpha_j(j-j')} \bar{A} \left(\alpha_m, \alpha_j, \frac{m+m'}{2}, \frac{j+j'}{2} \right). \quad (\text{A2})$$

Applying this to $\rho = \exp(-\mathbf{H}/k_B T)/Z$ yields Eq. (1) of the manuscript.

2. Initial Alignment

In order to estimate the initial alignment of a rotor in the potential $V(\beta) = -V_0 \cos^2 \beta$ we calculate the expectation value $\langle \cos^2 \beta \rangle_0 = \text{tr}(\rho_0 \cos^2 \beta)$. Inserting the initial state $\rho_0 = \exp(-\mathbf{H}/k_B T)/Z$ with $\mathbf{H} = \mathbf{J}^2/2I + V(\beta)$ shows that the expectation value can be expressed in terms of the partition function Z ,

$$\langle \cos^2 \beta \rangle_0 = k_B T \frac{\partial}{\partial V_0} \ln Z. \quad (\text{A3})$$

The latter can be calculated explicitly in the semiclassical limit, where the matrix elements of ρ_0 take the form (1),

$$Z = \sum_{j=0}^{\infty} \sum_{m=-j}^j \exp \left[-\frac{\hbar^2(j+1/2)^2}{2Ik_B T} \right] I_0 \left[\frac{V_0}{2k_B T} \left(1 - \frac{m^2}{(j+1/2)^2} \right) \right] \exp \left[\frac{V_0}{2k_B T} \left(1 - \frac{m^2}{(j+1/2)^2} \right) \right]. \quad (\text{A4})$$

One then replaces the sum over m by an integral from $-(j+1/2)$ to $+(j+1/2)$ and the sum over j by an integral over $j+1/2$. After the substitution $u = m/(j+1/2)$ we thus obtain

$$Z \simeq \frac{Ik_B T}{\hbar^2} \int_{-1}^1 du I_0 \left[\frac{V_0}{2k_B T} (1 - u^2) \right] \exp \left[\frac{V_0}{2k_B T} (1 - u^2) \right]. \quad (\text{A5})$$

The integral can be evaluated for $k_B T/V_0 \ll 1$ by using the asymptotic expansion $I_0(z) \sim e^z/\sqrt{2\pi z}$ as $z \rightarrow \infty$,

$$Z \simeq \frac{I(k_B T)^2}{\hbar^2 V_0} \exp \left(\frac{V_0}{k_B T} \right). \quad (\text{A6})$$

Inserting this into (A3) gives Eq. (2).

We remark that the same result (2) is obtained classically by calculating $\langle \cos^2 \beta \rangle_0$ with the marginal Boltzmann distribution of the polar angle β in the trap $f(\beta) = \sin \beta \exp(V_0 \cos^2 \beta/k_B T)/Z'$.

The total angular momentum expectation value of the initial distribution can be estimated with the semiclassical substitutions used above. In particular, carrying out the integral over m and subsuming the result into the new normalization Z' yields

$$\langle j \rangle_0 \simeq \frac{1}{Z'} \int_0^\infty dj j^2 \exp\left(-\frac{\hbar^2 j^2}{2Ik_B T}\right) = \sqrt{\frac{\pi Ik_B T}{2\hbar^2}}. \quad (\text{A7})$$

3. Classical Dispersion

We estimate the dispersion timescale by calculating the classical alignment loss of a Gaussian state released from the laser potential V_0 and approximating the rotor dynamics as flat. On a short timescale, the angle β evolves to $\beta(t) \simeq \beta + p_\beta t/I$, where p_β is the corresponding angular momentum. The marginal distribution of β and p_β follows from the Boltzmann distribution as $g(\beta, p_\beta) = \sin \beta \exp(-p_\beta^2/2Ik_B T + V_0 \cos^2 \beta/k_B T)/N$. With this one obtains the expectation value

$$\begin{aligned} \langle \cos^2 \beta \rangle_u &\simeq \int_0^\pi d\beta \int_{-\infty}^\infty dp_\beta g(\beta, p_\beta) \cos^2\left(\beta + \frac{p_\beta t}{I}\right) \\ &= \langle \cos^2 \beta \rangle_0 e^{-\kappa^2 t^2} + \frac{1}{2} \left(1 - e^{-\kappa^2 t^2}\right), \end{aligned} \quad (\text{A8})$$

with $\kappa = \sqrt{2k_B T/I}$.

4. Decoherence free alignment dynamics

The time-dependent alignment $\langle \cos^2 \beta \rangle_u$ due to the unitary dynamics is numerically calculated by carrying out the trace over the product of the time evolved state (4) and the operator-valued observable $\cos^2 \beta$. In particular, inserting Eq. (3) yields

$$\langle \cos^2 \beta \rangle_u = \sum_{j=0}^\infty \sum_{m=-j}^j \sum_{j'=0}^\infty \sum_{m'=-j'}^{j'} \langle jm | \rho_u(t) | j'm' \rangle \langle j'm' | \cos^2 \beta | jm \rangle, \quad (\text{A9})$$

where the matrix elements of $\rho_u(t)$ are given by Eq. (4) and

$$\langle jm | \cos^2 \beta | j'm' \rangle = \frac{\delta_{mm'}}{3} \left[(-1)^m 2\sqrt{(2j'+1)(2j+1)} \begin{pmatrix} j' & 2 & j \\ 0 & 0 & 0 \end{pmatrix} \begin{pmatrix} j' & 2 & j \\ m & 0 & -m \end{pmatrix} \delta_{mm'} + \delta_{jj'} \right] \quad (\text{A10})$$

Here, the angular bracket denote Wigner-3j symbols [D. M. Brink and G. Satchler, *Angular Momentum*, Oxford Science Publications, 2002]. Due to their selection rules, Eq. (A10) vanishes unless $j = j', j' \pm 2$, which significantly simplifies the evaluation of the alignment (5).

5. Orientational revivals of silicon nanorods

Figure 3 shows the alignment signal for silicon nanorods as discussed in the main text at a gas pressure of $p_g = 10^{-9}$ mbar. As in the case of carbon nanotubes, many revivals can be observed. The revival time is $T_{\text{rev}} = 28$ ms.

-
- [1] M. Aspelmeyer, T. J. Kippenberg, and F. Marquardt, *Rev. Mod. Phys.* **86**, 1391–1452 (2014).
[2] M. Arndt and K. Hornberger, *Nat. Phys.* **10**, 271–277 (2014).
[3] J. Teufel, T. Donner, D. Li, J. Harlow, M. Allman, K. Cicak, A. Sirois, J. D. Whittaker, K. Lehnert, and R. W. Simmonds, *Nature* **475**, 359–363 (2011).
[4] J. Chan, T. M. Alegre, A. H. Safavi-Naeini, J. T. Hill, A. Krause, S. Gröblacher, M. Aspelmeyer, and O. Painter, *Nature* **478**, 89–92 (2011).
[5] R. W. Peterson, T. P. Purdy, N. S. Kampel, R. W. Andrews, P.-L. Yu, K. W. Lehnert, and C. A. Regal, *Phys. Rev. Lett.* **116**, 063601 (2016).

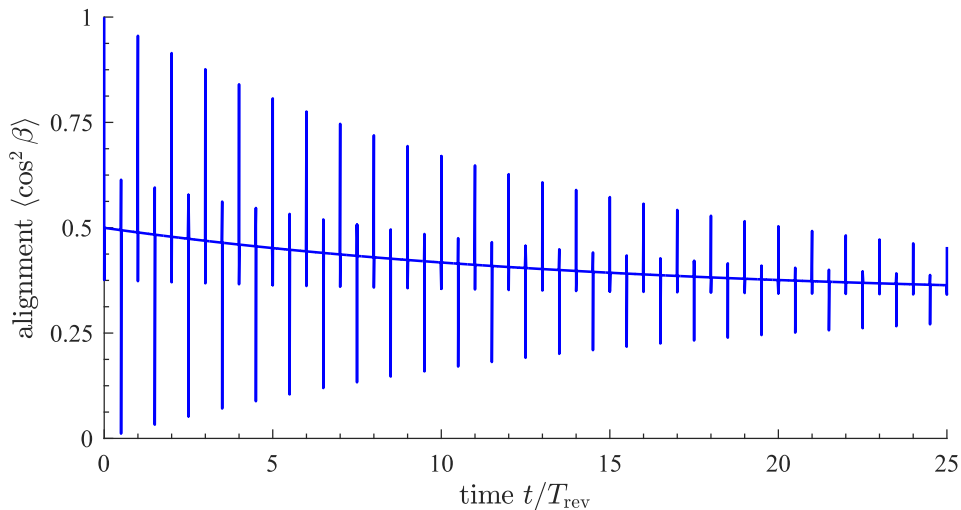


Figure 3. Orientational alignment $\langle \cos^2 \beta \rangle$ of the silicon nanorod discussed in the main text, as a function of time at $T = 100 \mu\text{K}$. For most of the times, the alignment signal decays exponentially with decoherence rate Γ from $1/2$ towards $1/3$. However, the initial alignment recurs at integer multiples of the revival time $T_{\text{rev}} = 2\pi I/\hbar$ and approaches a minimum at half integer multiples of T_{rev} .

- [6] D. Chang, C. Regal, S. Papp, D. Wilson, J. Ye, O. Painter, H. Kimble, and P. Zoller, *Proc. Natl. Acad. Sci. USA* **107**, 1005–1010 (2010).
- [7] O. Romero-Isart, M. L. Juan, R. Quidant, and J. I. Cirac, *New J. Phys.* **12**, 033015 (2010).
- [8] P. Barker and M. Shneider, *Physical Review A* **81**, 023826 (2010).
- [9] J. Gieseler, B. Deutsch, R. Quidant, and L. Novotny, *Phys. Rev. Lett.* **109**, 103603 (2012).
- [10] N. Kiesel, F. Blaser, U. Delić, D. Grass, R. Kaltenbaek, and M. Aspelmeyer, *Proc. Natl. Acad. Sci. USA* **110**, 14180–14185 (2013).
- [11] P. Asenbaum, S. Kuhn, S. Nimmrichter, U. Sezer, and M. Arndt, *Nat. Commun.* **4** (2013).
- [12] J. Millen, P. Fonseca, T. Mavrogordatos, T. Monteiro, and P. Barker, *Phys. Rev. Lett.* **114**, 123602 (2015).
- [13] P. Z. G. Fonseca, E. B. Aranas, J. Millen, T. S. Monteiro, and P. F. Barker, *Phys. Rev. Lett.* **117**, 173602 (2016).
- [14] J. Vovrosh, M. Rashid, D. Hempston, J. Bateman, M. Paternostro, and H. Ulbricht, *J. Opt. Soc. Am. B* **34**, 1421–1428 (2017).
- [15] G. Ranjit, M. Cunningham, K. Casey, and A. A. Geraci, *Phys. Rev. A* **93**, 053801 (2016).
- [16] D. C. Moore, A. D. Rider, and G. Gratta, *Phys. Rev. Lett.* **113**, 251801 (2014).
- [17] O. Romero-Isart, A. C. Pflanzner, F. Blaser, R. Kaltenbaek, N. Kiesel, M. Aspelmeyer, and J. I. Cirac, *Phys. Rev. Lett.* **107**, 020405 (2011).
- [18] J. Bateman, S. Nimmrichter, K. Hornberger, and H. Ulbricht, *Nat. Commun.* **5**, 4788 (2014).
- [19] B. A. Stickler, S. Nimmrichter, L. Martinetz, S. Kuhn, M. Arndt, and K. Hornberger, *Phys. Rev. A* **94**, 033818 (2016).
- [20] T. M. Hoang, Y. Ma, J. Ahn, J. Bang, F. Robicheaux, Z.-Q. Yin, and T. Li, *Phys. Rev. Lett.* **117**, 123604 (2016).
- [21] S. Kuhn, A. Kosloff, B. A. Stickler, F. Patolsky, K. Hornberger, M. Arndt, and J. Millen, *Optica* **4**, 356–360 (2017).
- [22] S. Kuhn, B. A. Stickler, A. Kosloff, F. Patolsky, K. Hornberger, M. Arndt, and J. Millen, *Nat. Commun.* **8**, 1670 (2017).
- [23] Z. Xu and T. Li, *Phys. Rev. A* **96**, 033843 (2017).
- [24] A. Manjavacas, F. J. Rodríguez-Fortuño, F. J. García de Abajo, and A. V. Zayats, *Phys. Rev. Lett.* **118**, 133605 (2017).
- [25] B. W. Shore, P. Dömötör, E. Sadurní, G. Süssmann, and W. P. Schleich, *New J. Phys.* **17**, 013046 (2015).
- [26] Y. Ma, T. M. Hoang, M. Gong, T. Li, and Z.-q. Yin, *Phys. Rev. A* **96**, 023827 (2017).
- [27] C. C. Rusconi and O. Romero-Isart, *Phys. Rev. B* **93**, 054427 (2016).
- [28] T. Delord, L. Nicolas, L. Schwab, and G. Hétet, *New J. Phys.* **19**, 033031 (2017).
- [29] S. Liu, T. Li, and Z.-q. Yin, *JOSA B* **34**, C8–C13 (2017).
- [30] K.-W. Xiao, N. Zhao, and Z.-q. Yin, *Phys. Rev. A* **96**, 013837 (2017).
- [31] T. Seideman, *Phys. Rev. Lett.* **83**, 4971 (1999).
- [32] M. D. Poulsen, E. Peronne, H. Stapelfeldt, C. Z. Bisgaard, S. S. Viftrup, E. Hamilton, and T. Seideman, *J. Chem. Phys.* **121**, 783–791 (2004).
- [33] T. Seideman and E. Hamilton, *Adv. At. Mol. Opt. Phys.* **52**, 289–329 (2005).
- [34] C. Zhong and F. Robicheaux, *Phys. Rev. A* **95**, 053421 (2017).
- [35] M. S. Child, *Semiclassical mechanics with molecular applications*, Oxford University Press, USA, 2014.
- [36] B. A. Stickler, B. Papendell, and K. Hornberger, *Phys. Rev. A* **94**, 033828 (2016).
- [37] C. Zhong and F. Robicheaux, *Phys. Rev. A* **94**, 052109 (2016).
- [38] B. Papendell, B. A. Stickler, and K. Hornberger, *New J. Phys.* **19**, 122001 (2017).
- [39] K. Hornberger, S. Uttenthaler, B. Brezger, L. Hackermüller, M. Arndt, and A. Zeilinger, *Phys. Rev. Lett.* **90**, 160401 (2003).

- [40] L. Hackermüller, K. Hornberger, B. Brezger, A. Zeilinger, and M. Arndt, *Nature* **427**, 711 (2004).
- [41] O. Romero-Isart, A. C. Pflanzer, M. L. Juan, R. Quidant, N. Kiesel, M. Aspelmeyer, and J. I. Cirac, *Phys. Rev. A* **83**, 013803 (2011).
- [42] H. Pino, J. Prat-Camps, K. Sinha, B. P. Venkatesh, and O. Romero-Isart, *Quant. Sci. Techn.* **3**, 025001 (2018).
- [43] S. Kuhn, P. Asenbaum, A. Kosloff, M. Sclafani, B. A. Stickler, S. Nimmrichter, K. Hornberger, O. Cheshnovsky, F. Patolsky, and M. Arndt, *Nano Lett.* **15**, 5604–5608 (2015).
- [44] K. Hansen and E. Campbell, *Phys. Rev. E* **58**, 5477 (1998).
- [45] B. Kozinsky and N. Marzari, *Phys. Rev. Lett.* **96**, 166801 (2006).
- [46] K. Liu, J. Deslippe, F. Xiao, R. B. Capaz, X. Hong, S. Aloni, A. Zettl, W. Wang, X. Bai, S. G. Louie, E. Wang, and F. Wang, *Nat. Nanotechn.* **7**, 325–329 (2012).
- [47] U. J. Kim, X. M. Liu, C. A. Furtado, G. Chen, R. Saito, J. Jiang, M. S. Dresselhaus, and P. C. Eklund, *Phys. Rev. Lett.* **95**, 157402 (2005).
- [48] S. Kuhn, G. Wachter, F.-F. Wieser, J. Millen, M. Schneider, J. Schalko, U. Schmid, M. Trupke, and M. Arndt, *Appl. Phys. Lett.* **111**, 253107 (2017).
- [49] A. Bassi, K. Lochan, S. Satin, T. Singh, and H. Ulbricht, *Rev. Mod. Phys.* **85**, 471–527 (2013).
- [50] B. Schriniski, B. A. Stickler, and K. Hornberger, *J. Opt. Soc. Am. B* **34**, C1–C7 (2017).